



A robust 3D fast spin-echo technique for fast examination of the brachial plexus

Daehyun Yoon¹ · Neha Antil¹ · Sandip Biswal¹ · Amelie M. Lutz¹ 

Received: 5 October 2021 / Revised: 17 February 2022 / Accepted: 17 February 2022 / Published online: 26 March 2022
© ISS 2022

Abstract

Objective To introduce a 3D fast spin-echo (FSE) sequence technique that may replace conventional clinical 2D FSE sequences for examining the brachial plexus.

Materials and methods A 3D FSE sequence with motion-sensitized driven equilibrium magnitude preparation, triple-echo Dixon, and outer-volume suppression techniques, dubbed as MSDE-CUBE-fTED, was compared with clinical 2D T2-weighted and T1-weighted FSE sequences on the conventional brachial plexus exam of 14 volunteers. The resulting images were evaluated by two radiologists for fat suppression, blood flow suppression, nerve visualization, scalene muscle shape, surrounding fat planes, and diagnostic confidence. The inter-rater agreement of the reviewers was also measured. In addition, the signal magnitude ratios and contrast-to-noise ratios between nerve-to-vessel, nerve-to-muscle, and fat-to-muscle were compared.

Results The MSDE-CUBE-fTED sequence scored significantly higher than the T2-weighted FSE sequence in all visualization categories ($P < 0.05$). Its score was not significantly different from that of the T1-weighted FSE in muscle and fat visualization ($P \geq 0.5$). The inter-rater agreements were substantial (Gwet's agreement coefficient ≥ 0.7). The signal magnitude and contrast ratios were significantly higher in the MSDE-CUBE-fTED sequence ($P < 0.05$).

Conclusion Our results suggest that the MSDE-CUBE-fTED sequence can make a potential alternative to standard T2- and T1-weighted FSE sequences for examining the brachial plexus.

Keywords MSDE · 3D FSE · Peripheral nerve · Brachial plexus

Introduction

MRI has been increasingly used as a noninvasive examination of the brachial plexus [1–3]. The bright fat contrast of the T1-weighted fast spin-echo (T1w-FSE) images has facilitated the identification of major anatomic structures and secondary muscular changes from denervation. The water-only T2-w FSE images have been used for the detection of the signal increase of the peripheral nerve possibly due to pathologic changes. However, the brachial plexus MRI poses a few challenges that should be addressed for a reliable examination [4, 5]. The homogeneous suppression of fat to acquire the water-only T2-weighted contrast is often problematic because of strong-off resonance around

the neck. Avoiding the phase wrapping artifacts along with the left–right direction results in a substantial increase of the scan time due to the large shoulder-to-shoulder body volume. Non-suppressed vessel signal can be a problem, predominantly in evaluating small branches of the brachial plexus. This is because it can be challenging to differentiate between small veins and nerves with pathologically increased T2 signals [6].

A few different 3D imaging approaches have been recently developed to address each of the aforementioned issues in imaging the brachial plexus. A 3D diffusion-weighted steady-state sequence showed encouraging results in suppressing the blood flow signal [7], but its contrast and motion robustness were somewhat weak [8]. A 3D FSE sequence with a modified Dixon approach and low refocusing flip angles demonstrated better fat–water separation and blood flow signal attenuation than the 3D short-tau inversion recovery (STIR) FSE sequence [9]. However, its blood flow signal suppression through adjusting the refocusing flip angle was suspected to be less effective

✉ Amelie M. Lutz
alutz@stanford.edu

¹ Radiology, Stanford University, Stanford, CA 94305, USA

than a direct blood flow signal suppression technique such as the motion-sensitized driven equilibrium (MSDE) technique [10]. A 3D FSE sequence with MSDE preparation significantly improved contrast between nerves and blood vessels [11–13], but they adopted STIR for fat suppression, which penalizes signal-to-noise ratio (SNR) compared to the Dixon-based fat–water separation methods. Therefore, there is still a need for a novel MRI pulse sequence that can offer the improved visualization of the brachial plexus with a clinically feasible scan time.

In this work, we present a robust 3D FSE technique for the brachial plexus exam that incorporates the fast spin-echo triple-echo Dixon technique (fTED) [14], the MSDE magnitude preparation [15], and the outer-volume suppression, which, respectively, provides robust fat–water separation, improved nerve-vessel distinction, and reduced scan time. The goal of our research is to determine whether our proposed sequence may be equivalent to or better than standard 2D FSE sequences in the conventional clinical brachial plexus exam. Particularly, we focused on comparing the in-phase and water-only images between our sequence, the 2D T1w-FSE sequence, and the 2D T2-w FSE sequence with the two-point Dixon method (T2w-FSE-FLEX). We conducted a qualitative image review and quantitative contrast measurements to compare the nerve and muscle visualization qualities between these sequences.

Material and methods

Proposed 3D sequence

The structure of the proposed 3D FSE sequence, dubbed as MSDE-CUBE-fTED, is briefly presented in Fig. 1. The

sequence begins with two magnitude preparation modules: (1) MSDE module with a composite RF pulse for robustness to B0 and B1 inhomogeneities [15], which was interleaved by motion sensitizing gradient waveforms to suppress blood flow signal [16], and (2) outer-volume suppression module with a train of high bandwidth (8 kHz) RF pulses to bilaterally saturate the magnetization outside the prescribed phase-FOV [17]. Then, a 3D FSE pulse train for signal acquisition begins where the refocusing pulses are modulated with a variable flip angle schedule for reduced SAR and image blurring [18]. The triple-echo readout with consecutive gradients of alternating polarity was adopted to implement the fast spin-echo triple-echo Dixon technique for robust fat–water separation [14].

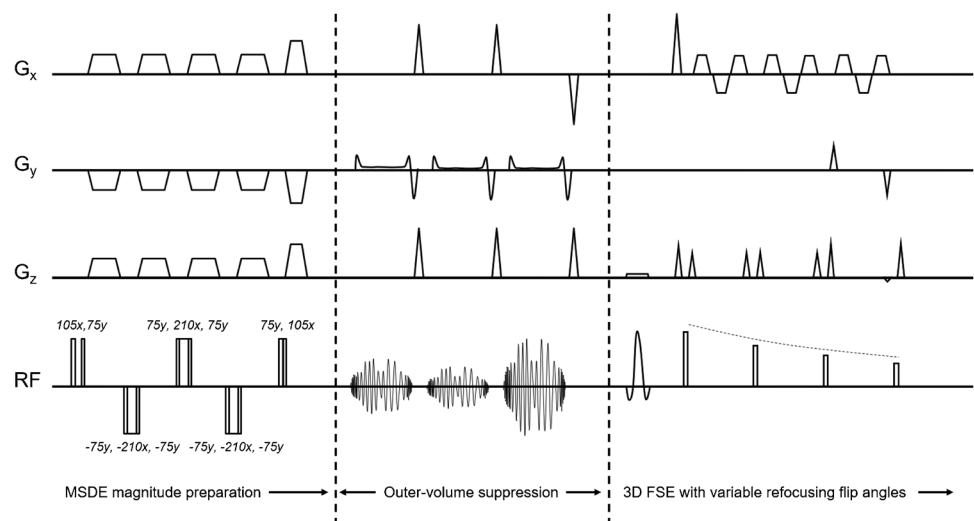
Subject participation

This study was approved by the institutional review board for Health Insurance Portability and Accountability Act (HIPPA) compliance. The subjects were recruited among those patients referred for brachial plexus MRI in our clinics. For the patients who consented to participate in our study, the proposed MSDE sequence was appended to the clinical brachial plexus MRI protocol for data collection. Fourteen subjects participated (eight men, six women; mean age 40 years, with a range of 16–67 years). Subjects with general contraindications for MRI, such as claustrophobia and MRI-incompatible devices, were excluded from recruitment.

MRI scans

All MRI acquisition was conducted on a 3T GE MRI scanner (Discovery MR750, GE Healthcare, Waukesha, USA) with an HNS head/neck/chest phased coil array with 13 channels

Fig. 1 Pulse sequence diagram of the proposed MSDE-CUBE-fTED. This is a 3D FSE sequence using variable refocusing pulse flip angles (CUBE) and triple-echo readout (fTED) with two magnitude preparation modules: (1) motion-sensitized driven equilibrium (MSDE) magnitude preparation with a composite pulse train and (2) bilateral outer-volume suppression with high bandwidth (8 kHz) RF pulse trains



for signal reception. Images from the MSDE-CUBE-fTED sequence were acquired on the coronal imaging plane and compared with those from 2D coronal T2w-FSE-FLEX and 2D sagittal T1w-FSE sequences. The pulse sequence parameters are introduced in Table 1. In the MSDE module of the MSDE-CUBE-fTED sequence, the size of the gradient for blood flow suppression was characterized by calculating the associated velocity encoding (VENC) value. The lower VENC value has a better blood flow signal suppression capability than the higher VENC values, at the increased risk of creating eddy current artifacts. After a few test scans, we found 1.7 cm/s VENC achieves reasonable blood flow signal suppression without noticeable signal loss artifacts due to eddy currents. The magnetization outside the phase-encode FOV (32.4 cm, left to right direction) was saturated with outer-volume suppression.

Image assessment

Two musculoskeletal radiologists (AL with 18 years of experience and NA 6 years of experience in interpreting brachial plexus MRI scans) scored the water images from the MSDE-CUBE-fTED and T2w-FSE-FLEX sequences on a 3-point scale for four qualitative categories (fat suppression, vessel suppression, nerve visualization, and diagnostic confidence). These reviewers were not blinded to the type of source sequences associated with the images. However, the images were reviewed separately after a 2-week time interval and in changing the order of the different patients. We have considered removing the sequence information before the review, but the image characteristics of the proposed 3D MSDE sequence were distinctive such that the reviewers could easily identify the source sequences in the blinded preliminary evaluations. They also scored the in-phase MSDE-CUBE-fTED images reformatted on the sagittal plane to directly compare with the sagittal

T1w-FSE images for three categories (scalene muscle shape, surrounding fat planes, diagnostic confidence) on a 3-point scale. The changes of muscle bulk and inter/intra-muscular fat are structural markers associated with potential edema and denervation, and T1-weighted images are commonly used to identify them. In our study, we focused on the analysis of the scalene muscle as an example for the regional muscle evaluation because, in addition to the above pathologic changes, we also often encounter structural variants in its origins and attachments, which can lead to a deviation of some brachial plexus nerve roots. In the diagnostic confidence category, we attempted to evaluate the overall scan quality and visibility of the imaged anatomy and whether the readers think that they can make diagnostic calls about abnormal findings on the exams in their daily clinical practice. This was categorized into 0 for not confident at all, 1 for moderately confident, and 2 for very confident. For the image quality parameters, 0 stood for non-diagnostic, 1 for moderate but diagnostic, and 2 for excellent and diagnostic.

Signal magnitude ratios (SMR) and contrast-to-noise ratios (CNR) between nerve, muscle, fat, and blood vessels were also measured for quantitative comparison. To calculate SMR and CNR, small ROIs were first drawn by DY under the guidance of AL on the C7 spinal nerve, scalene muscle, suprascapular vein, and subcutaneous fat of the compared sequence images. In-phase images were used for the SMR and CNR of fat-to-muscle calculation, and water-only images were used to calculate the SMRs and CNR of other tissues. The mean of magnitude signal within the ROI was then measured. The following equations were used to finally derive the SMR and CNR.

$$\text{SMR of A-to-B} = \frac{\text{Mean magnitude signal of A}}{\text{Mean magnitude signal of B}}$$

$$\text{CNR of A-to-B} = \frac{\text{Mean magnitude signal of A} - \text{Mean magnitude signal of B}}{\text{Standard deviation of background air space}}$$

Table 1 Pulse sequence parameters of the compared MSDE-CUBE-fTED, T2w-FSE-FLEX, and T1w-FSE sequences

	MSDE-CUBE-fTED	T2w-FSE-FLEX	T1w-FSE
TR	2.5 s	7.6 s	0.83 s
TE	60 ms	54 ms	14.4 ms
Echo train length	64	14	4
FOV (frequency × phase × slice)	36 × 32.4 × 26 cm	22 × 22 × 11.9 cm	18 × 18 × 21 cm
In-plane image size (frequency × phase)	288 × 260	384 × 224	512 × 224
Slice thickness	2 mm	3 mm	4 mm
Slice spacing	0	0.3 mm	1 mm
Bandwidth	± 250 kHz	± 50 kHz	± 35.71 kHz
Undersampling factor (phase × slice)	2 × 2	2 × 1	1 × 1
Number of excitation	1	2	2
No phase wrap	No	Yes	Yes
Scan time	5 min 8 s	4 min 59 s	6 min 19 s

Statistical analysis

The image review scores for each category were compared using the two-tailed Wilcoxon signed-rank test, and the SMR and CNR were compared in the same fashion. The significance level was set to be 5% for rejecting the null hypothesis that the compared sequences do not have a significant difference. The inter-rater agreement of the two reviewers on the review scores was assessed using Gwet's agreement coefficient [19].

Results

Review scores

The MSDE-CUBE-fTED sequence scored significantly higher than the clinical T2w-FSE-FLEX sequence in all qualitative evaluation categories, as summarized in Fig. 2A. The mean \pm standard deviation of review scores from MSDE-CUBE-fTED and T2w-FSE-FLEX sequences were 2.00 ± 0.00 and 1.50 ± 0.50 for fat suppression, 1.40 ± 0.49 and 0.89 ± 0.31 for vessel suppression, 1.96 ± 0.19 and 1.32 ± 0.47 for nerve visualization, and 2.00 ± 0.00 and 1.57 ± 0.49 for diagnostic confidence. The associated *P* values were less than 0.01. Gwet's agreement coefficients were 1.0 (fat suppression), 0.7 (vessel suppression), 0.9 (nerve visualization), and 0.7 (diagnostic confidence). There was no significant difference between the review scores of the MSDE-CUBE-fTED sequence and the clinical T1w-FSE sequence in any evaluation category, as plotted in Fig. 2B. The mean \pm standard deviation of review scores between MSDE-CUBE-fTED and T1w-FSE sequences were 1.89 ± 0.31 and 1.89 ± 0.31 for scalene muscle shape, 1.82 ± 0.38 and 1.89 ± 0.31 for surrounding fat planes, and 1.93 ± 0.26 and 1.89 ± 0.31 for diagnostic

confidence. The associated *P* values were 1 (scalene muscle shape), 0.5 (surrounding fat planes), and 1 (diagnostic confidence). Gwet's agreement coefficients were 0.8 (scalene muscle shape), 0.7 (surrounding fat planes), and 0.8 (diagnostic confidence).

SMR and CNR

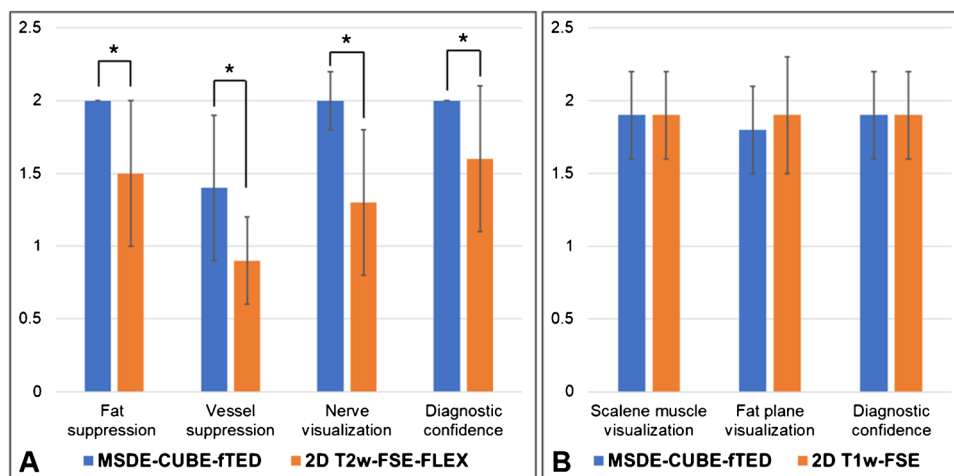
The MSDE-CUBE-fTED sequence achieved significantly higher SMR than the clinical 2D FSE sequences, as illustrated in Fig. 3A. The mean \pm standard deviation of SMR from the proposed sequence and 2D FSE sequence images were 1.7 ± 0.4 and 1.4 ± 0.3 for nerve-to-muscle ratio, 3.5 ± 1.2 and 2.0 ± 0.9 for nerve-to-vessel ratio, and 3.6 ± 0.9 and 2.6 ± 0.4 for fat-to-muscle ratio. The associated *P* values were 0.04 (nerve-to-muscle ratio), 0.01 (nerve-to-vessel ratio), and 0.01 (fat-to-muscle ratio).

The CNR of the MSDE-CUBE-fTED sequence was also significantly higher than those of compared FSE sequences in all categories, as shown in Fig. 3B. The mean \pm standard deviation of CNR from our sequence and 2D FSE sequences were 59.9 ± 27.2 and 16.1 ± 8.3 for nerve-to-muscle contrast, 88.6 ± 29.3 and 21.9 ± 17.4 for nerve-to-vessel contrast, and 169.4 ± 96.5 and 51.4 ± 27.6 for fat-to-muscle contrast. The associated *P* values were all less than 0.01.

Case examples

Figures 4 and 5 present examples of improved nerve visualization and blood signal suppression by the proposed MSDE-CUBE-fTED sequence compared to the T2w-FSE-FLEX sequence. Figure 6 demonstrates the comparable visualization quality of the scalene muscle and fat planes between the MSDE-CUBE-fTED image and the conventional T1w-FSE image.

Fig. 2 Review scores of water images (A) and in-phase images (B) between the MSDE-CUBE-fTED, 2D T2w-FSE-FLEX, and 2D T1w-FSE sequences. The water images of the MSDE-CUBE-fTED sequence scored significantly higher (* mark: $P < 0.05$) than T2w-FSE-FLEX water images in all review categories. There was no significant difference ($P > 0.5$) between the scores of in-phase images in any category



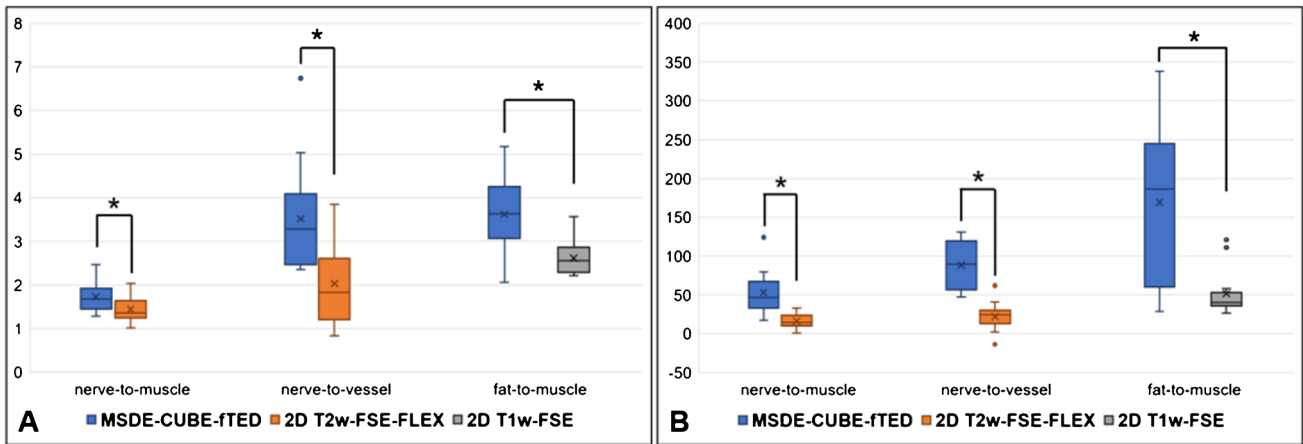
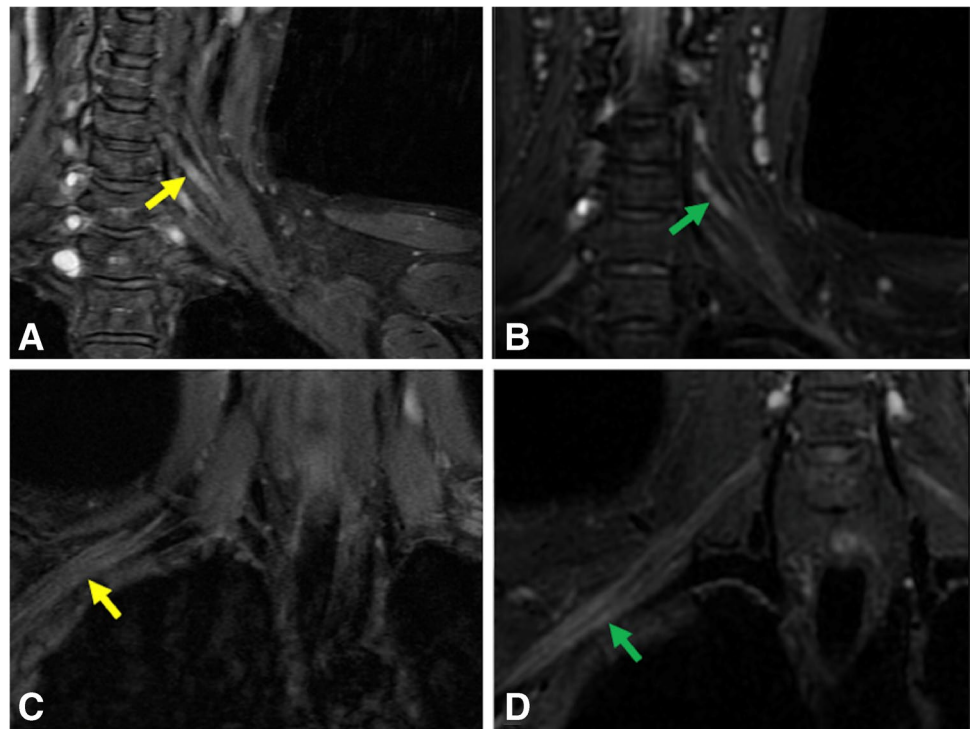


Fig. 3 SMR (A) and CNR (B) of nerve-to-muscle, nerve-to-vessel, and fat-to-muscle between the compared sequences. The SMR and CNR of the proposed MSDE-CUBE-ftED images were higher than those of clinical 2D FSE images in all categories (* mark: $P < 0.05$)

Fig. 4 Improved nerve visualization by the MSDE-CUBE-ftED sequence compared to T2w-FSE-FLEX. **A** (T2w-FSE-FLEX) and **B** (MSDE-CUBE-ftED) are from one subject, and **C** (T2w-FSE-FLEX) and **D** (MSDE-CUBE-ftED) are from another subject. The peripheral nerves of the brachial plexus on the source T2w-FSE-FLEX water images (**A**, **C**) blend in with the surrounding musculature showing subtle contrast between musculature and abnormal plexus elements (yellow arrows). However, the source images from the MSDE-CUBE-ftED sequence (**B**, **D**) show a more striking signal contrast between peripheral nerves (green arrows) and surrounding musculature



Discussion

In this study, we compared the MSDE-CUBE-ftED sequence with clinical 2D T2w-FSE-FLEX and 2D T1w-FSE sequences by conducting a qualitative radiologic review and quantitative contrast measurements of the brachial plexus images from fourteen volunteers. The MSDE-CUBE-ftED water images demonstrated significantly higher review scores in fat–water separation, nerve visualization, and vessel suppression than T2w-FSE-FLEX water

images. We suppose the slight increase of the fat–water separation quality in the MSDE-CUBE-ftED might be due to the adoption of the fast triple-echo Dixon approach. It measures in-phase and out-of-phase signals at each echo, while the in-phase and out-of-phase signal acquisitions are interleaved by a TR (7.6 s) in the 2D T2w-FSE-FLEX sequence. Therefore, the in-phase and out-of-phase images of the MSDE-CUBE-ftED sequence have a lower chance of misregistration with each other, which might help the subsequent fat–water separation process. The 75%

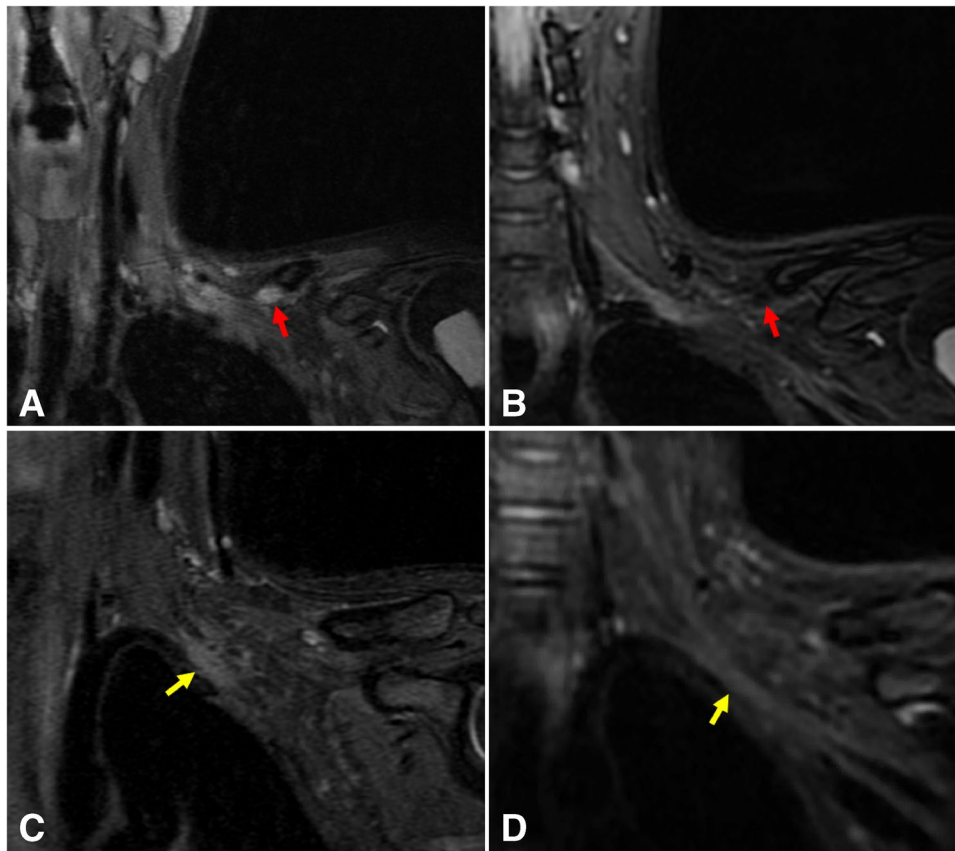


Fig. 5 Improved suppression of blood vessel signal on the proposed sequence compared to T2w-FSE-FLEX. **A** T2w-FSE-FLEX and **B** MSDE-CUBE-fTED are from one subject, and **C** T2w-FSE-FLEX and **D** MSDE-CUBE-fTED are from another subject. For each case, the most comparable slices were chosen to mitigate the slight difference of the imaging axis and slice thickness between the two sequences. The signal from the suprascapular vein in the infraclavicular region (red arrows) is quite strong on the T2w-FSE-FLEX image

(**A**), while it is well suppressed on the image of the MSDE-CUBE-fTED sequence (**B**, red arrow). On the T2w-FSE-FLEX image (**C**), adjacent subclavian vessel walls are often difficult to separate from the brachial plexus structures (yellow arrow), whereas on the image of the MSDE-CUBE-fTED sequence (**D**, yellow arrow), this does not pose a problem due to the robust vessel signal suppression and thinner slice thickness, reducing partial volume effects

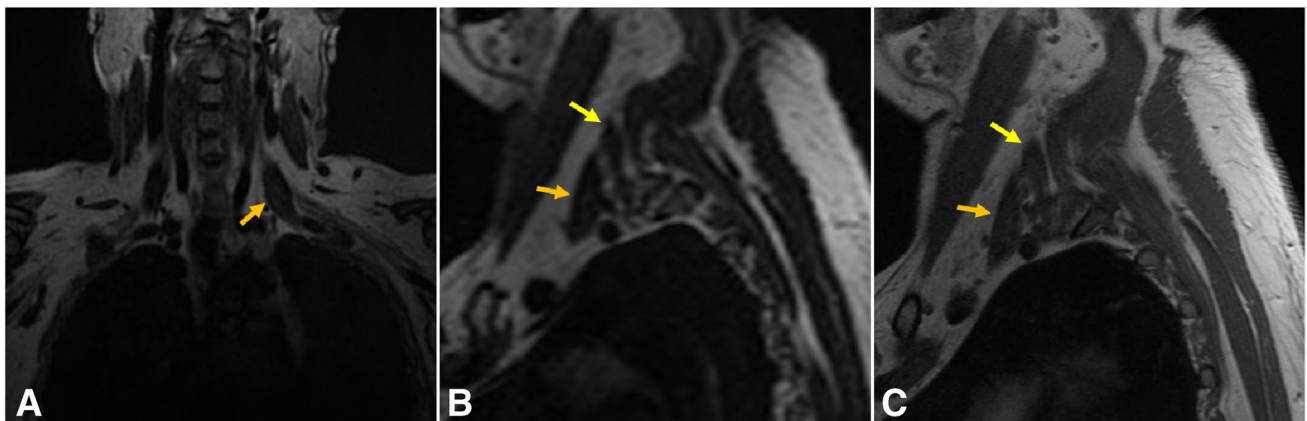


Fig. 6 Demonstrates the comparable fat-to-muscle contrast between the in-phase image on the original coronal imaging plane from the MSDE-CUBE-fTED sequence (**A**), the reformatted in-phase image on the sagittal plane (**B**), and the sagittal T1w-FSE image (**C**). Both **A** and **B** demonstrate excellent contrast between fat and muscle tissue,

comparable to that of clinical standard sequence (**C**). This muscle-fat contrast is an important feature when evaluating anatomic variants and the relationship between the anterior scalene muscle (orange arrows) and the middle scalene muscle (yellow arrows) as well as the brachial plexus

increase of the nerve-to-vessel SMR of the MSDE-CUBE-ftED sequence can be attributed to the MSDE magnitude preparation pulse. The MSDE preparation can be adopted in the 2D T2w-FSE-FLEX, but the associated SAR deposition will be much higher than the 3D FSE sequence because the preparation should be applied for each slice acquisition. This will likely increase the TR and thus elongate the scan time significantly. The nerve-to-muscle CNR increase by the MSDE-CUBE-ftED sequence was substantially high compared to that of the 2D T2w-FSE-FLEX sequence (59.9 vs 16.1). The larger voxel volume (3.13 mm³ vs 1.68 mm³) contributed to this, but even after the normalization by the voxel volume, the nerve-to-muscle CNR of the MSDE-CUBE-ftED sequence was still 100% higher. We suppose the baseline SNR boost by the noise averaging effect of the 3D acquisition is likely the main source of the CNR increase.

The overall contrast of the MSDE-CUBE-ftED in-phase images and the T1w-FSE images was not identical, with the MSDE-CUBE-ftED sequence showing a slightly higher fat-to-muscle contrast. However, the scores of MSDE-CUBE-ftED in-phase images were comparable to those of T1w-FSE images in the visualization of the scalene muscles and surrounding fat plane shapes, suggesting they may also suffice in the evaluation of muscle anatomy, including muscle bulk, muscle variant anatomy, and fat plane visibility. Note that, in our setup, the in-plane resolution of the MSDE-CUBE-ftED image reformatted on the sagittal plane was not as high as that of the T1w-FSE; however, it was sufficient to identify the bulk shape and major boundaries of scalene muscle components, subcutaneous fat layers, and background fat planes. We expect that the sequence may achieve a comparable resolution on the reformatted images with the further development of isotropic high-resolution acquisition schemes. The higher review scores of the MSDE-CUBE-ftED images than the clinical FSE sequences were coherently observed in both reviewers' evaluation results, possibly due to more details from thinner slices thickness.

Our approach has a few limitations. The adopted fat–water separation approach of the proposed sequence requires fast switching of the readout gradient for achieving a high resolution in the frequency-encoding direction. The maximum achievable resolution under the current hardware limitation was 1.25 mm, which needs to be further improved to help the quality of the original acquisition as well as the reformats. We expect the resolution improvement can be implemented with a better gradient system and additional data sampling of the gradient ramp period. The suppression of the slow blood flow signal was limited in the adopted MSDE preparation scheme because the required high amplitude gradient to dephase the slow blood flow signal also caused eddy current–induced signal loss artifacts. Post-contrast STIR imaging recently demonstrated the promise

for vascular signal suppression less dependent on the speed of the blood flow [20]. This approach may be considered an alternative if the risk associated with the gadolinium contrast injection is acceptable. The small size of the subject population and lack of clinical outcomes at the time of the study made it very challenging to validate identified imaging abnormalities. A further longitudinal study of a larger patient group will be followed to evaluate the clinical utility of the imaging findings as well as the development of high-resolution isotropic imaging for more flexible reformats.

Conclusion

In summary, the MSDE-CUBE-ftED sequence was presented, which demonstrated improved visualization of the brachial plexus over the background muscles and blood vessels compared to the clinical 2D T2w-FSE-FLEX sequence. It also achieved comparable visualization of the muscles and background fat planes to the clinical 2D T1w-FSE sequence. The results indicate that the proposed sequence has a strong potential to facilitate the accelerated exam of the brachial plexus with overall improved visualization qualities.

Acknowledgements We thank Dr. Jarrett Rosenberg for the assistance with statistical processing. This work was supported by GE Healthcare and NIH P41 EB015891.

Funding This study was supported by GE Healthcare and NIH P41 EB015891.

Declarations

Ethics approval All procedures performed in studies involving human participants were in accordance with the ethical standards of the institutional and/or national research committee and with the 1964 Helsinki declaration and its later amendments or comparable ethical standards.

Conflict of interest Daehyun Yoon received research support from GE Healthcare regarding the development of the presented work. The remaining authors, Neha Antil, Sandip Biswal, and Amelie Lutz, have no conflict of interest.

References

1. Aagaard BD, Maravilla KR, Kliot M. MR neurography. MR imaging of peripheral nerves. *Magn Reson Imaging Clin N Am*. 1998;6(1):179–94.
2. Du R, Auguste KI, Chin CT, Engstrom JW, Weinstein PR. Magnetic resonance neurography for the evaluation of peripheral nerve, brachial plexus, and nerve root disorders. *J Neurosurg*. 2010;112(2):362–71.
3. van Rosmalen MHJ, Goedee HS, van der Gijp A, Witkamp TD, van Eijk RPA, Asselman FL, et al. Quantitative assessment of

- brachial plexus MRI for the diagnosis of chronic inflammatory neuropathies. *J Neurol*. 2021;268(3):978–88.
4. Maravilla KR, Bowen BC. Imaging of the peripheral nervous system: evaluation of peripheral neuropathy and plexopathy. *AJNR Am J Neuroradiol*. 1998;19(6):1011–23.
 5. Chhabra A, Andreisek G, Soldatos T, Wang KC, Flammang AJ, Belzberg AJ, et al. MR neurography: past, present, and future. *AJR Am J Roentgenol*. 2011;197(3):583–91.
 6. Chhabra A, Zhao L, Carrino JA, Trueblood E, Koceski S, Shteriev F, et al. MR neurography: advances. *Radiol Res Pract*. 2013;2013:809568.
 7. Zhang Z, Meng Q, Chen Y, Li Z, Luo B, Yang Z, et al. 3-T imaging of the cranial nerves using three-dimensional reversed FISP with diffusion-weighted MR sequence. *J Magn Reson Imaging*. 2008;27(3):454–8.
 8. Chhabra A, Subhawong TK, Bizzell C, Flammang A, Soldatos T. 3T MR neurography using three-dimensional diffusion-weighted PSIF: technical issues and advantages. *Skeletal Radiol*. 2011;40(10):1355–60.
 9. Wang X, Harrison C, Mariappan YK, Gopalakrishnan K, Chhabra A, Lenkinski RE, et al. MR neurography of brachial plexus at 3.0 T with robust fat and blood suppression. *Radiology*. 2017;283(2):538–46.
 10. Wang J, Yarnykh VL, Yuan C. Enhanced image quality in black-blood MRI using the improved motion-sensitized driven-equilibrium (iMSDE) sequence. *J Magn Reson Imaging*. 2010;31(5):1256–63.
 11. Yoneyama M, Takahara T, Kwee TC, Nakamura M, Tabuchi T. Rapid high resolution MR neurography with a diffusion-weighted pre-pulse. *Magn Reson Med Sci*. 2013;12(2):111–9.
 12. Kasper JM, Wadhwa V, Scott KM, Rozen S, Xi Y, Chhabra A. SHINKEI—a novel 3D isotropic MR neurography technique: technical advantages over 3DIRTSE-based imaging. *Eur Radiol*. 2015;25(6):1672–7.
 13. Klupp E, Cervantes B, Sollmann N, Treibel F, Weidlich D, Baum T, et al. Improved brachial plexus visualization using an adiabatic iMSDE-prepared STIR 3D TSE. *Clin Neuroradiol*. 2019;29(4):631–8.
 14. Ma J, Son JB, Zhou Y, Le-Petross H, Choi H. Fast spin-echo triple-echo Dixon (fTED) technique for efficient T2-weighted water and fat imaging. *Magn Reson Med*. 2007;58(1):103–9.
 15. Brittain JH, Hu BS, Wright GA, Meyer CH, Macovski A, Nishimura DG. Coronary angiography with magnetization-prepared T2 contrast. *Magn Reson Med*. 1995;33(5):689–96.
 16. Taviani V, Mitsuhashi M, Wang K, King K, Banerjee S, Biswal S, et al. A flexible technique for flow-sensitive fat-suppressed high-resolution peripheral nerve imaging. *Proc Int Soc Magn Reson Med*. 2017:96.
 17. Banerjee S, Han M, Chen W, Hess CP, Krug R, Shankaranarayanan A, et al. Reduced field-of-view imaging with 3D variable flip angle fast spin echo—feasibility in MRI of orbits. *Proc Int Soc Magn Reson Med*. 2015:2309.
 18. Busse RF, Brau AC, Vu A, Michelich CR, Bayram E, Kijowski R, et al. Effects of refocusing flip angle modulation and view ordering in 3D fast spin echo. *Magn Reson Med*. 2008;60(3):640–9.
 19. Gwet KL. Computing inter-rater reliability and its variance in the presence of high agreement. *Br J Math Stat Psychol*. 2008;61(Pt 1):29–48.
 20. Sneag DB, Daniels SP, Geannette C, Queler SC, Lin BQ, de Silva C, et al. Post-contrast 3D inversion recovery magnetic resonance neurography for evaluation of branch nerves of the brachial plexus. *Eur J Radiol*. 2020;132:109304.

Publisher's note Springer Nature remains neutral with regard to jurisdictional claims in published maps and institutional affiliations.